Vortex structures in a rotating Rydberg-dressed Bose-Einstein condensate with the Lee-Huang-Yang correction

Che-Hsiu Hsueh,* Ching-Wei Wang,* and Wen-Chin Wu†
Department of Physics, National Taiwan Normal University, Taipei 11677, Taiwan

(Received 6 October 2020; accepted 20 November 2020; published 4 December 2020)

We numerically investigate the vortex structures in a fast rotating two-dimensional Rydberg-dressed Bose-Einstein condensate (BEC) taking into account the Lee-Huang-Yang (LHY) quantum correction. In a rotating BEC of reduced dimensionality, it is shown that there is room to tune the LHY coupling against the short- and long-range couplings. In the absence of the LHY effect, hexagonal, square, striped, and honeycomb lattices can exhibit upon increasing the long-range interaction, which can be realized in the context of superfluid (SF)-supersolid (SS) transition. In the presence of the LHY effect, competition between LHY and long-range terms results in rich lattice structures. In particular, clustering of multiple vortices can occur due to the trapping effect of the SS triangles or grids. Estimates of number of vortices in the clustering are provided.

DOI: 10.1103/PhysRevA.102.063307

I. INTRODUCTION

In 1957, Abrikosov published a classic paper on magnetic vortices in type-II superconductors and predicted the vortex lattices to be hexagonal close packing (HCP) [1,2]. It then inspired people to investigate the vortex lattice structures in various superconducting and superfluid (SF) systems. Pioneering works in rotating SF include studies of vortex lattices in superfluid helium [3,4] and cold atoms [5,6].

Supersolid (SS) is a state of matter that simultaneously possesses superfluidity and solidity in which both gauge and continuous translational symmetries are broken [7–12]. To maintain global phase coherence in the SF background, spontaneous density modulation associated with SF-SS transition then arises [13–16]. Recently SS states have been realized in a spin-orbit coupling Bose-Einstein condensate (BEC) in the stripe phase [17], and in optical cavities coupled BEC [18]. Moreover, crystallization of SS with the help of long-range interaction has also been detected in dipolar BEC [16,19–21]. Another promising candidate to observe the SS state is the Rydberg-dressed atomic BEC which exhibits a defocusing soft-core interaction [22–26].

Lee-Huang-Yang (LHY) quantum correction is considered the first correction beyond the mean-field approximation in SF systems [27]. In dipolar BECs, energy of the LHY term is repulsive and $\propto n^{5/2}$ (n being the atom density), whereas due to anisotropy of the dipolar interaction, energy of the dipolar interaction could be attractive and $\propto n^2$. Competition of the two terms then finds a ground state to form self-bound droplets [20,28–32]. By contrast, in Rydberg-dressed BECs, the long-range interaction is isotropic and the system can stabilize itself and form a SS in the absence of the LHY correction. Nevertheless, the higher-order LHY effect could still play some interesting roles in Rydberg-dressed BEC. Recently the effect of LHY correction on ground-state properties [16,33,34] and excitation spectra [34–36] have been investigated in Rydberg-dressed BEC. The present paper aims to explore how the vortex structures behave with the LHY effect in Rydberg-dressed BECs under high rotation.

In a three-dimensional (3D) Rydberg-dressed BEC, LHY coupling is completely bounded by the short (g) and long-range (α) couplings, so there is not much room to adjust the LHY coupling once g and α are fixed. However, in a two-dimensional (2D) geometry of particular interest for vortex lattices, there occurs an additional dependence of l_z (condensate size along the rotation axis). Consequently due to the different-power dependence of l_z on the LHY term versus the short- and long-range terms, it gives room to adjust the LHY coupling against the short- and long-range couplings (see Sec. II). This in turn makes rich vortex structures in a 2D system.

In the literature, Henkel *et al.* [37] studied rotating SS and presented a phase diagram for the competition between SS crystal and rotation-induced vortex lattice in a Rydberg-dressed BEC. Cheng and Jheng [38] studied the von Neumann vortex lattices in a BEC with dipole interatomic interaction. Kwasigroch and Cooper [39] studied quantum fluctuations of vortex lattices in ultracold gases by a variational method. Kumar *et al.* [40] studied vortex lattices in binary BEC with dipolar interaction. Tengstrand *et al.* [41] studied rotating binary BEC and vortex clusters in quantum droplets. Tamil Thiruvalluvar *et al.* [42] studied vortex formation and vortex lattices in a BEC with LHY correction. Roccuzzo *et al.* [43] studied rotating SS in a dipolar gas with LHY correction. Gallemí *et al.* [44] investigated quantized vortices in dipolar SS BEC with LHY correction. In an earlier paper, Sinova *et al.* [45] studied quantum melting and absence of BEC in 2D vortex matter.

The paper is organized as follows. Section II introduces the basic formalism of the Gross-Pitaevskii equation (GPE)

*These authors contributed equally to this work.
†wu@ntnu.edu.tw

with the LHY correction. Section III studies the vortex lattices in a 2D rotating Rydberg-dressed BEC in the absence of LHY correction. Section IV studies the vortex structures in a 2D rotating Rydberg-dressed BEC with the LHY correction. Section V is a conclusion. In Appendix, a derivation for the lattice constant of the hexagonal trapped Rydberg-dressed SS is given.

II. FORMALISM

This paper takes the approach of GPE. In a three-dimensional Rydberg-dressed BEC, condensed atoms interact with each other via the following potential [22]:

$$U(\mathbf{r}-\mathbf{r}') = g\delta(\mathbf{r}-\mathbf{r}') + \frac{\alpha}{R_c^6 + |\mathbf{r}-\mathbf{r}'|^6}, \tag{1}$$

where $g = 4\pi\hbar^2 a/m$ (a being the s-wave scattering length) is responsible for the short-range interaction and α and R_c are the van der Waals interaction strength and blockade radius of the long-range interaction. The sound velocity of the system is then given by

$$c(\mathbf{r}) = \sqrt{\frac{g_{\rm eff} n(\mathbf{r})}{m}}, \tag{2}$$

where $n(\mathbf{r})$ is local density, m is atom mass, and $g_{\rm eff}$ is the effective coupling given by

$$g_{\rm eff} = \tilde{U}(\mathbf{k}=0) = g + \frac{2\pi^2\alpha}{3R_c^3} \tag{3}$$

with $\tilde{U}(\mathbf{k})$ the Fourier transform of $U(\mathbf{r})$ in (1). Under local density approximation, the energy functional of the LHY correction is given by [27]

$$E_{\rm LHY} = \frac{8m^4}{15\pi^2\hbar^3}\int c(\mathbf{r})^5 d\mathbf{r} = \frac{2}{5}\gamma\int |\psi(\mathbf{r})|^5 d\mathbf{r}, \tag{4}$$

where the LHY coupling $\gamma = 4m^{\frac{3}{2}} g_{\rm eff}^{\frac{5}{2}}/3\pi^2\hbar^3$ and the total wave function $\psi(\mathbf{r})$ is subject to the normalization condition $\int |\psi(\mathbf{r})|^2 d\mathbf{r} = 1$. Consequently the total energy functional of the system is [46]

$$E = \int\left[\frac{\hbar^2|\nabla\psi(\mathbf{r})|^2}{2m} + \frac{m\omega_\perp^2(\rho^2+\lambda^2 z^2)}{2}|\psi(\mathbf{r})|^2 + \frac{g}{2}|\psi(\mathbf{r})|^4 + \frac{\alpha}{2}\int\frac{|\psi(\mathbf{r}')|^2|\psi(\mathbf{r})|^2}{R_c^6+|\mathbf{r}-\mathbf{r}'|^6}d\mathbf{r}' + \frac{2}{5}\gamma|\psi(\mathbf{r})|^5\right]d\mathbf{r}, \tag{5}$$

where $\rho^2 = x^2+y^2$, $\omega_\perp$ (ω_z) is the trapping frequency in the x-y plane (along the z axis), and $\lambda = \omega_z/\omega_\perp$ is the aspect ratio.

In a two-dimensional geometry confining to the x-y plane ($\lambda \gg 1$), total wave function $\psi(\mathbf{r},t) \approx \phi(\vec{\rho},t)\bar{\phi}(z)$, where $\vec{\rho} = (x,y)$ and the z-component wave function can be well approximated by a Gaussian,

$$\bar{\phi}(z) = \frac{1}{\pi^{1/4} l_z^{1/2}}\exp\left(-\frac{z^2}{2l_z^2}\right), \tag{6}$$

with $l_z = \sqrt{\hbar/m\omega_z}$. In the case $R_c \gg l_z$ appropriate for the 2D limit, the long-range term in (5) can then be approximated by

$$\iint\frac{|\psi(\mathbf{r}')|^2|\psi(\mathbf{r})|^2}{R_c^6+|\mathbf{r}-\mathbf{r}'|^6}d\mathbf{r}'d\mathbf{r} \approx \frac{1}{\sqrt{2\pi}l_z}\iint\frac{|\phi(\vec{\rho}')|^2|\phi(\vec{\rho})|^2}{R_c^6+|\vec{\rho}-\vec{\rho}'|^6}d\vec{\rho}'d\vec{\rho}. \tag{7}$$

Consequently the total energy functional (5) is reduced to

$$E = \int\left[\frac{\hbar^2|\nabla_\perp\phi(\vec{\rho})|^2}{2m} + \frac{m\omega_\perp^2\rho^2}{2}|\phi(\vec{\rho})|^2 + \frac{g}{2\sqrt{2\pi}l_z}|\phi(\vec{\rho})|^4 + \frac{\alpha}{2\sqrt{2\pi}l_z}\int\frac{|\phi(\vec{\rho}')|^2|\phi(\vec{\rho})|^2}{R_c^6+|\vec{\rho}-\vec{\rho}'|^6}d\vec{\rho}' + \left(\frac{2}{5}\right)^{\frac{3}{2}}\frac{\gamma}{\pi^{\frac{3}{4}}l_z^{\frac{3}{2}}}|\phi(\vec{\rho})|^5 + \frac{\hbar\omega_z}{2}\right]d\vec{\rho}. \tag{8}$$

Considering a rotation around the z axis, the total energy functional in the rotating frame is then

$$E_{\rm rot} = E - \Omega\int\phi^*(\vec{\rho})\hat{L}_z\phi(\vec{\rho})d\vec{\rho}, \tag{9}$$

where Ω is the angular frequency of rotation and $\hat{L}_z$ is the z-component angular momentum. Based on (9), one can write down a corresponding time-dependent 2D GPE with the LHY correction:

$$i\hbar\partial_t\phi(\vec{\rho}) = \left[-\frac{\hbar^2\nabla_\perp^2}{2m} + \frac{m\omega_\perp^2\rho^2}{2} + \bar{g}|\phi(\vec{\rho})|^2 + \bar{\alpha}\int\frac{|\phi(\vec{\rho}')|^2}{R_c^6+|\vec{\rho}-\vec{\rho}'|^6}d\vec{\rho}' + \bar{\gamma}|\phi(\vec{\rho})|^3 - \Omega L_z\right]\phi(\vec{\rho}). \tag{10}$$

Here $\bar{g} = g/\sqrt{2\pi}l_z$, $\bar{\alpha} = \alpha/\sqrt{2\pi}l_z$, and $\bar{\gamma} = \sqrt{2/5}\gamma/\pi^{\frac{3}{4}}l_z^{\frac{3}{2}}$. Thus $\bar{g}/g = \bar{\alpha}/\alpha \propto l_z^{-1}$, whereas $\bar{\gamma}/\gamma \propto l_z^{-\frac{3}{2}}$. As a matter of fact, due to the different-power dependence of l_z on $\bar{\gamma}$ versus $\bar{g}$ and $\bar{\alpha}$, it gives room to adjust the LHY coupling against the short- and long-range couplings Throughout this paper, the units of length and frequency are chosen to be the blockade radius R_c and the characteristic frequency associated with R_c, $\omega_c = \hbar/mR_c^2$, respectively.

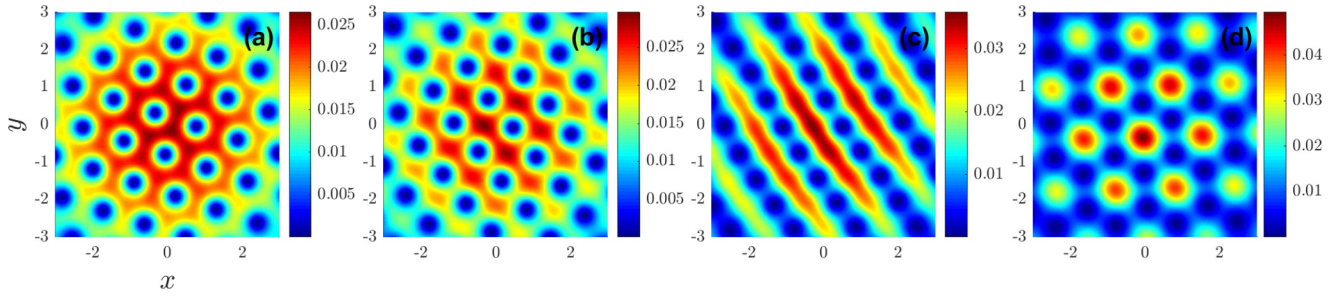

FIG. 1. Vortex lattices of a fast rotating 2D Rydberg-dressed condensate without LHY correction. $R_{\rm TF} = 7R_c$, $\omega_\perp = 3\omega_c$, $\Omega = 0.95\omega_\perp = 2.85\omega_c$, and $\bar{g}_{\rm eff} = 1655$ are used in all frames. All axes are in units of R_c. Upon decreasing (increasing) the short-range (long-range) coupling $\bar{g}$ ($\bar{\alpha}$), it exhibits (a) hexagonal ($\bar{g} = 200$; $\bar{\alpha} = 383$), (b) square ($\bar{g} = 150$; $\bar{\alpha} = 397$), (c) striped ($\bar{g} = 63$; $\bar{\alpha} = 420$), and (d) honeycomb ($\bar{g} = 38$; $\bar{\alpha} = 426$) lattices.

The stationary lattice configurations discussed in the rest of this paper are obtained by evolving Eq. (10) in imaginary time. Fast Fourier transformation (FFT) and inverse fast Fourier transformation (IFFT) are employed to deal with spatial difference and integration [47]. We discretized the two-dimensional calculating domain $(-4\pi, 4\pi) \times (-4\pi, 4\pi)$ to 384×384 grids. Besides, the time-splitting method with a fixed time step $\Delta t = 0.001$ is used to deal with temporal difference and integration. The "ground states" we obtained are very robust against the using of the spatially random trial wave functions and the convergence criterium of chemical potential.

III. VORTEX LATTICES WITHOUT LHY CORRECTION

It is useful to first examine vortex lattices in the absence of LHY correction ($\bar{\gamma} = 0$). Under Thomas-Fermi (TF) approximation, the TF radius of the rotating 2D condensate is given by

$$R_{\rm TF} = \sqrt{\frac{2\mu}{m(\omega_\perp^2 - \Omega^2)}} = \sqrt{\frac{2\bar{g}_{\rm eff} n_0}{m(\omega_\perp^2 - \Omega^2)}}, \tag{11}$$

where μ is the chemical potential and $n_0 = 2/\pi R_{\rm TF}^2$ is the normalized number density maximum at $\rho = 0$. The 2D effective coupling,

$$\bar{g}_{\rm eff} = \tilde{U}_{\rm 2D}(\mathbf{k}_\parallel = 0) = \bar{g} + \frac{2\pi^2\bar{\alpha}}{3\sqrt{3}R_c^4}, \tag{12}$$

where $\tilde{U}_{\rm 2D}(\mathbf{k}_\parallel)$ is the Fourier transform of the 2D potential involving both short- and long-range interactions,

$$U_{\rm 2D}(\vec{\rho}) = \bar{g}\delta(\rho) + \frac{\bar{\alpha}}{R_c^6 + \rho^6}. \tag{13}$$

Equation (11) also reveals

$$\bar{g}_{\rm eff} = \frac{m(\omega_\perp^2 - \Omega^2)\pi R_{\rm TF}^4}{4}, \tag{14}$$

so $\bar{g}_{\rm eff}$ is fixed once $\omega_\perp$, Ω, and $R_{\rm TF}$ are fixed.

Figure 1 shows vortex lattices of a fast rotating 2D Rydberg-dressed condensate without LHY correction. We consider a large condensate of $R_{\rm TF} = 7R_c$ and $\omega_\perp = 3\omega_c$, which is under fast rotation with $\Omega = 0.95\omega_\perp = 2.85\omega_c$. Based on (14), it yields $\bar{g}_{\rm eff} = 1655$. With $\bar{g}_{\rm eff}$ fixed and by varying relative magnitudes of $\bar{g}$ and $\bar{\alpha}$ [see (12)], four distinct vortex lattices are observed. Given Fig. 1, the smaller $\bar{g}$ (or the larger $\bar{\alpha}$) is, the condensate lines more anisotropically which spontaneously breaks continuous translational symmetry and finally conforms to the hexagonal, square, striped, and honeycomb vortex lattices. Recently numerical results of honeycomb vortex lattice have been found in dipolar SS BEC [32,44].

Vortices correspond to local energy or density minima in the ground state. In the current system, condensate with large $R_{\rm TF}$ can accommodate more vortices and high rotation frequency Ω can generate large angular momentum. Starting from the case of uniform SF where vortex lattice exhibits to be hexagonal close packing [case (a)], vortices are distorted into a square pattern due to the increasing weight of the long-range interaction [case (b)]. As long-range interaction increases further, there is the first-order transition from square to the anisotropic striped lattice [case (c)] until the striped lattice finally transforms into the honeycomb lattice commensurate with the hexagonal SS structure [case (d)] [37]. Evolution of vortex lattices in which vortices accommodate in the valleys of condensate density can thus be deemed as the SF-SS transition [44].

IV. VORTEX STRUCTURES WITH LHY CORRECTION

Figure 2 shows vortex structures of a fast rotating 2D Rydberg-dressed condensate with LHY correction. Following Fig. 1, we again consider a large condensate with $R_{\rm TF} = 7R_c$ and $\omega_\perp = 3\omega_c$, which is under fast rotation with $\Omega = 0.95\omega_\perp = 2.85\omega_c$. As shown in (12) and (14) and also noted before, the effective coupling $\bar{g}_{\rm eff}$, which is the combination of the short-range $\bar{g}$ and long-range $\bar{\alpha}$ couplings, is fixed once $R_{\rm TF}$, $\omega_\perp$, and Ω are set. The above $R_{\rm TF}$, $\omega_\perp$, and Ω used yield $\bar{g}_{\rm eff} = 1655$.

Figure 2 intends to study the competition between long-range coupling $\bar{\alpha}$ and LHY coupling $\bar{\gamma}$. For simplicity, we fix $\bar{g} = 0$ and $\bar{\alpha} = 436$ (a combination also corresponding to $\bar{g}_{\rm eff} = 1655$) and vary $\bar{\gamma}$. Later in Figs. 4 and 5, we will take the same approach to turn off the short-range coupling $\bar{g}$ by considering the effects of higher rotation frequencies. The effect of $\bar{g}$ will be studied and discussed in Fig. 7.

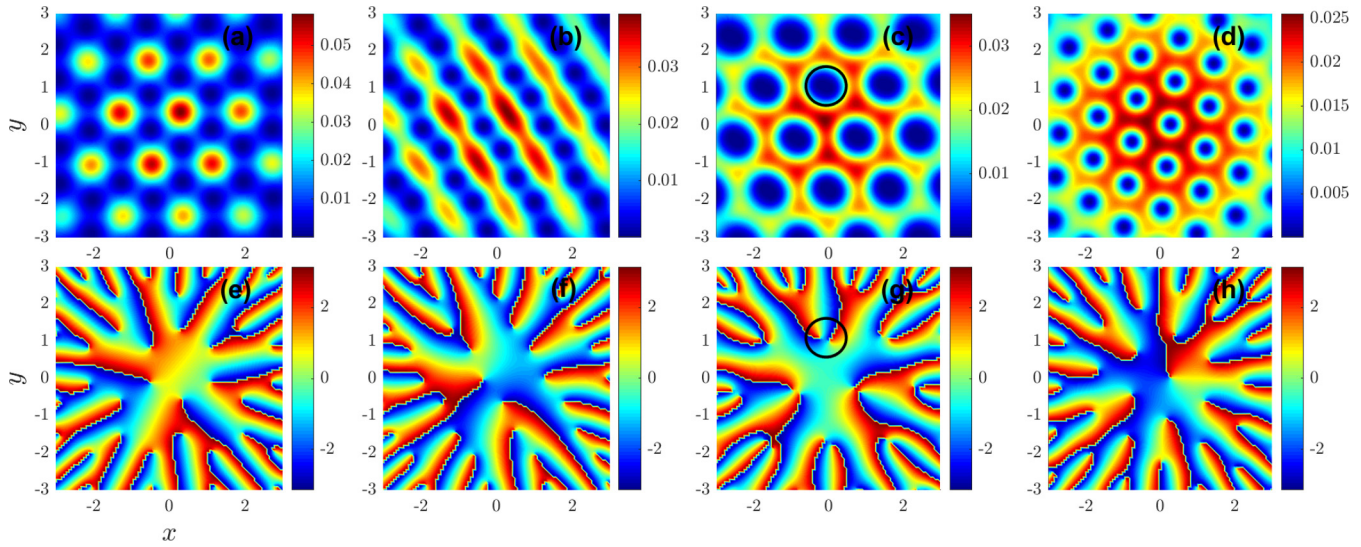

FIG. 2. (a)–(d) Vortex structures of a fast rotating 2D Rydberg-dressed condensate with LHY correction $\bar{\gamma}$. $R_{\rm TF} = 7R_c$, $\omega_\perp = 3\omega_c$, $\Omega = 0.95\omega_\perp = 2.85\omega_c$, and $\bar{g}_{\rm eff} = 1655$ with $\bar{g} = 0$ and $\bar{\alpha} = 436$ are used in all frames. All axes are in units of R_c. Upon increasing $\bar{\gamma}$, it exhibits (a) honeycomb lattice ($\bar{\gamma} = 0$), (b) striped lattice ($\bar{\gamma} = 200$), (c) clustering of paired vortices in a hexagonal structure ($\bar{\gamma} = 260$), and (d) hexagonal lattice ($\bar{\gamma} = 1000$). (e)–(h) Corresponding to the phase distributions of (a)–(d). The clustering of paired vortices in (c) is confirmed by the circle in (g).

Analogous to the one in Fig. 1(d) with relatively larger $\bar{\alpha} = 426$ and smaller $\bar{g} = 38$, a honeycomb lattice is also observed in Fig. 2(a) for $\bar{\gamma} = 0$. Upon increasing the LHY coupling $\bar{\gamma}$, Fig. 2 also shows (b) striped lattice ($\bar{\gamma} = 200$), (c) clustering of paired vortices in a hexagonal structure ($\bar{\gamma} = 260$), and (d) hexagonal lattice ($\bar{\gamma} = 1000$).

A. Roton instability

Energy of LHY term is $\propto \bar{\gamma}|\phi|^5$ [see (8)]. It implies when $\bar{\gamma}$ is increased, a higher local density would cost more energy and consequently, SS could transform towards the SF phase with a more flat and uniform density distribution. To see how SS would transform towards the SF state by increasing the LHY coupling, we study the phenomenon of roton instability. Based on Bogoliubov-de Gennes (BdG) equation, the excitation spectrum of a 2D *uniform* Rydberg-dressed LHY condensate can be given by

$$\hbar\omega(\mathbf{k}_\parallel) = \pm\sqrt{\frac{\hbar^2 k_\parallel^2}{2m}\left[\frac{\hbar^2 k_\parallel^2}{2m} + 2\tilde{U}_{\rm 2D}(\mathbf{k}_\parallel)n_0 + 3\bar{\gamma}n_0^{\frac{3}{2}}\right]}, \quad (15)$$

where n_0 is the 2D uniform density and $\tilde{U}_{\rm 2D}(\mathbf{k})$ is the Fourier transform of the 2D interaction potential given in (13). At $\mathbf{k}_\parallel \to 0$, the excitation dispersion is phononlike,

$$\omega = ck_\parallel; \quad c = c_0\left[1 + \frac{3\bar{\gamma}n_0^{\frac{1}{2}}}{2\bar{g}_{\rm eff}}\right]^{\frac{1}{2}}, \quad (16)$$

where $c_0 = \sqrt{\bar{g}_{\rm eff}n_0/m}$ and $\bar{g}_{\rm eff}$ was given in (12).

Figure 3 shows roton instability occurs in a case with $\bar{\alpha}n_0 = 100$ and $\bar{\gamma}n_0^{3/2} = 0$ (solid blue curve). When $\bar{\gamma}$ is increased while $\bar{\alpha}n_0$ is fixed at 100, excitation dispersion is raised and eventually, roton instability is lifted (dashed green curve). It indicates the SS state can transform towards the homogeneous SF state.

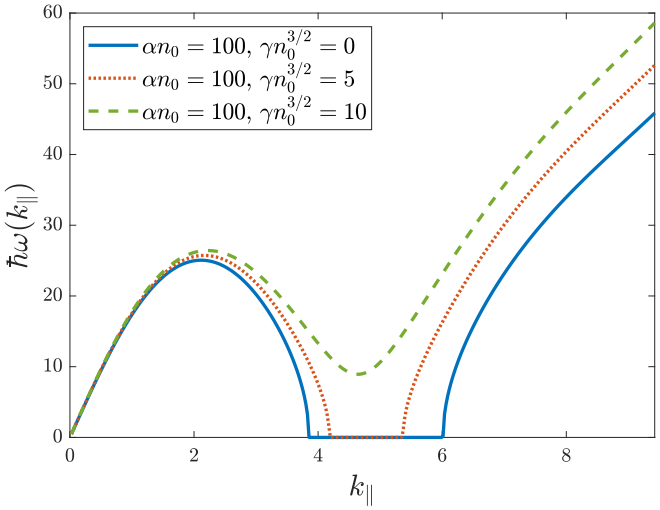

FIG. 3. Schematic showing the effect of LHY correction on the BdG excitation spectra (15). With the long-range coupling $\bar{\alpha}$ and density n_0 fixed, roton instability is lifted by increasing the LHY coupling $\bar{\gamma}$.

B. Clustering of multiple vortices

Figure 2(c) exhibits the clustering of paired vortices of the same circulation [40,48], as confirmed by the corresponding phase distribution in Fig. 2(g) (see the circle). By contrast, vortex lattices in Figs. 2(a), 2(b), and 2(d) are all made up of a single vortex.

In fact, clustering of multiple vortices can occur in both small and intermediate $\bar{\gamma}$ regimes. For small $\bar{\gamma}$'s, the vortex

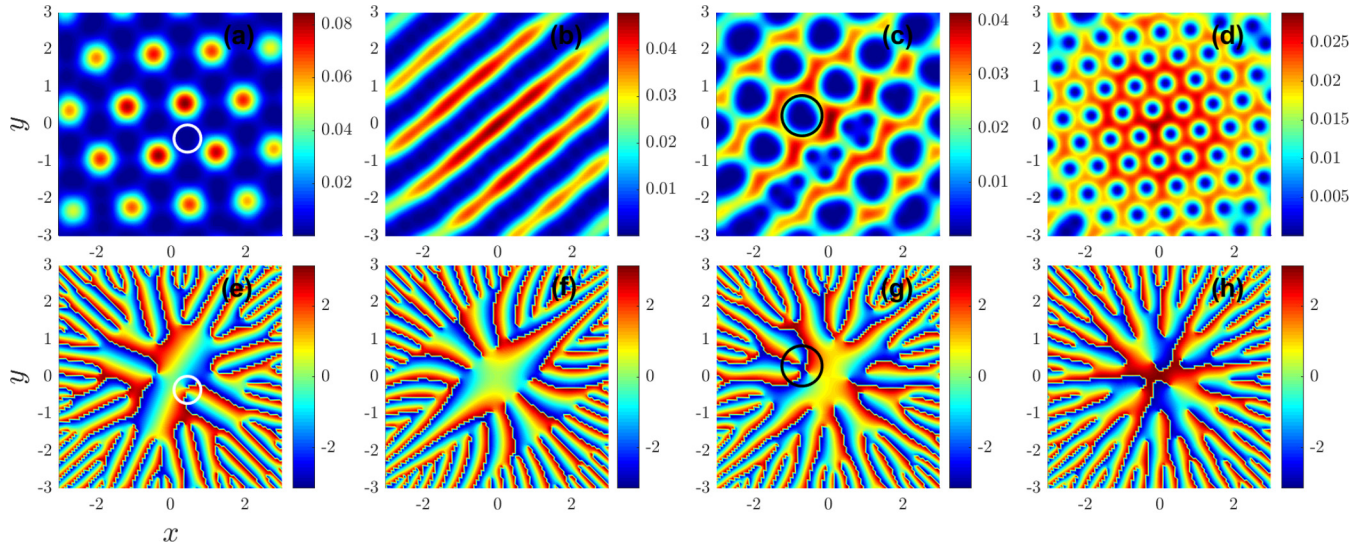

FIG. 4. (a)–(d) Vortex structures of a fast rotating 2D Rydberg-dressed condensate with LHY correction $\bar{\gamma}$. $R_{\rm TF} = 6R_c$, $\omega_\perp = 6\omega_c$, $\Omega = 0.95\omega_\perp = 5.7\omega_c$, and $\bar{g}_{\rm eff} = 3573$ with $\bar{g} = 0$ and $\bar{\alpha} = 941$ are used in all frames. All axes are in units of R_c. Upon increasing $\bar{\gamma}$, it exhibits (a) clustering of paired vortices in a honeycomb structure ($\bar{\gamma} = 300$), (b) striped lattice ($\bar{\gamma} = 600$), (c) clustering of three vortices in a hexagonal structure ($\bar{\gamma} = 990$), and (d) hexagonal lattice ($\bar{\gamma} = 1100$). (e)–(h) Corresponding to the phase distributions of (a)–(d).

structure is a honeycomb in the background of hexagonal SS [Fig. 2(a)]. Let n_1 denote the number of vortices trapped in a triangle formed by three nearby droplets of the hexagonal SS. Assume that a is the lattice constant of the hexagonal SS and the area of triangle is $\mathcal{A}_\triangle = \sqrt{3}a^2/4$. In Appendix, we have shown $a \approx \pi R_{\rm c}/2$ for the hexagonal Rydberg-dressed SS under studies. Consequently $\mathcal{A}_\triangle \approx (\sqrt{3}\pi^2/16)R_c^2 \approx 1.07$. On the other hand, based on the lowest Landau level (LLL) approximation for a fast rotating condensate [49], each vortex takes up an averaged area $\mathcal{A}_{\rm LLL} = \pi\ell^2$ with $\ell = \sqrt{\hbar/m\Omega}$ and Ω the rotation frequency. We have found empirically that

$$n_1 \approx \text{Rounding}\left[\frac{\mathcal{A}_\triangle}{\mathcal{A}_{\rm LLL}}\right] \approx \text{Rounding}\left[\frac{\sqrt{3}\pi R_{\rm c}^2 m\Omega}{16\hbar}\right], \quad (17)$$

where Rounding $[x]$ denotes rounding to the nearest integer. In the present case, $\Omega = 2.85\omega_\perp$, it yields $\mathcal{A}_{\rm LLL} \approx 1.10$ and $\mathcal{A}_\triangle/\mathcal{A}_{\rm LLL} \approx 0.97$. Consequently, $n_1 = 1$.

When $\bar{\gamma}$ is increased, SS droplets start to get flattened and connect first to form linear arrays [Fig. 2(b)]. By the linear SS arrays, vortices then form single-vortex lines (stripes) in the density-low regions. The lattice constant of the stripes

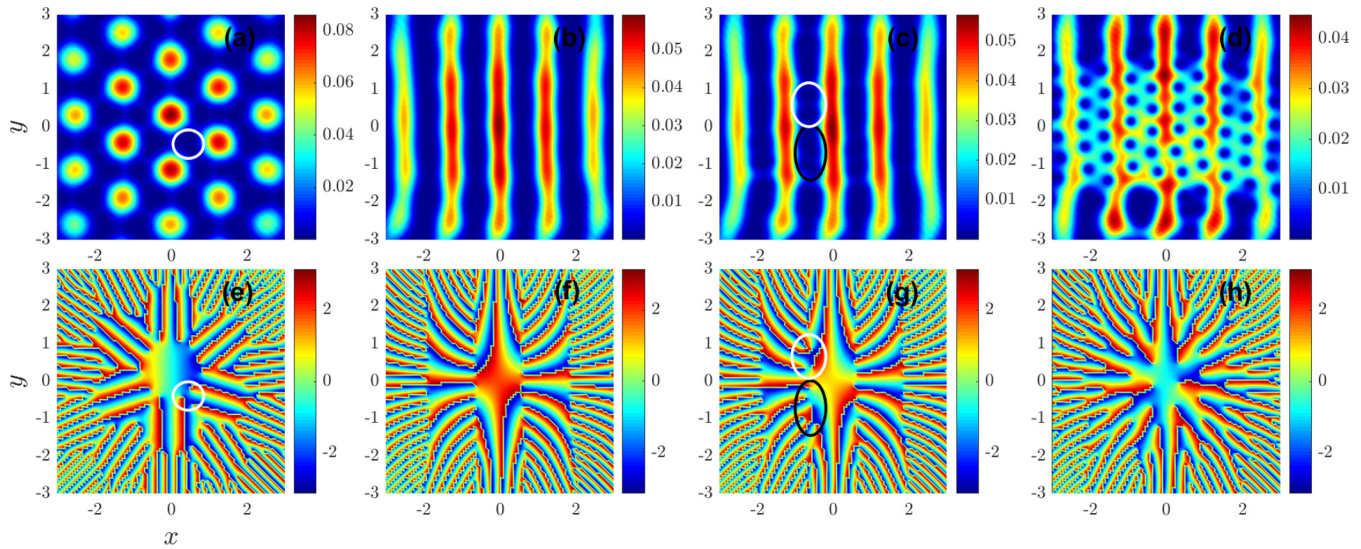

FIG. 5. (a)–(d) Vortex structures of a fast rotating 2D Rydberg-dressed condensate with LHY correction $\bar{\gamma}$. $R_{\rm TF} = 6R_c$, $\omega_\perp = 9.29\omega_c$, $\Omega = 0.95\omega_\perp = 8.82\omega_c$, and $\bar{g}_{\rm eff} = 8579$ with $\bar{g} = 0$ and $\bar{\alpha} = 2260$ are used in all frames. All axes are in units of R_c. Upon increasing $\bar{\gamma}$, it exhibits (a) clustering of three vortices in a honeycomb structure ($\bar{\gamma} = 1250$), (b) striped lattice ($\bar{\gamma} = 1500$), (c) clustering of four (see the white oval) or five (see the black oval) vortices in a linear structure ($\bar{\gamma} = 1805$), and (d) hexagonal lattice mixed with the striped SS ($\bar{\gamma} = 1810$). (e)–(h) Corresponding to the phase distributions of (a)–(d).

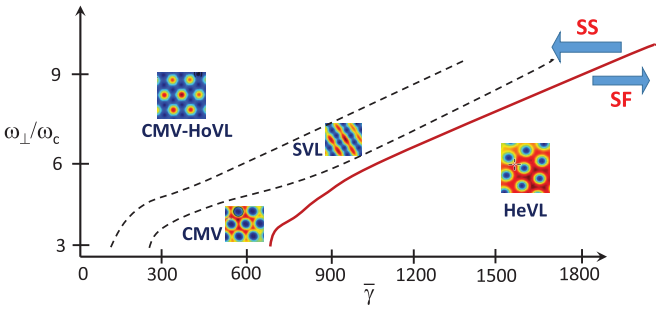

FIG. 6. Phase diagram of the vortex structures for a fast rotating 2D Rydberg-dressed condensate with LHY correction $\bar{\gamma}$. CMV-HoVL denotes clustering of multiple vortices in a honeycomb vortex lattice, SVL denotes the striped vortex lattice, CMV denotes clustering of multiple vortices either in hexagonal or linear structure, and HeVL denotes the hexagonal vortex lattice.

(shortest distance between two neighboring stripes) is $a' = \sqrt{3}a/2 \approx \sqrt{3}\pi R_c/4$. When $\bar{\gamma}$ is increased further, SS gets further flattened and extends also to the direction perpendicular to the stripes. Consequently a SS grid structure can form and each grid has an area $\mathcal{A}_\square = (a')^2 = 3a^2/4 \approx 3\pi^2 R_c^2/16$. The number of vortices trapped in a single SS grid, named n_2, is found to be

$$n_2 \approx \text{Rounding}\left[\frac{\mathcal{A}_\square}{\mathcal{A}_{\text{LLL}}}\right] \approx \text{Rounding}\left[\frac{3\pi R_c^2 m\Omega}{16\hbar}\right]. \quad (18)$$

In the present case, $\mathcal{A}_\square \approx 1.85$ and $\mathcal{A}_\square/\mathcal{A}_{\text{LLL}} \approx 1.68$, thus $n_2 = 2$. This is what is seen in Fig. 2(c) in which paired vortices tend to form a hexagonal structure in a closed-packing manner.

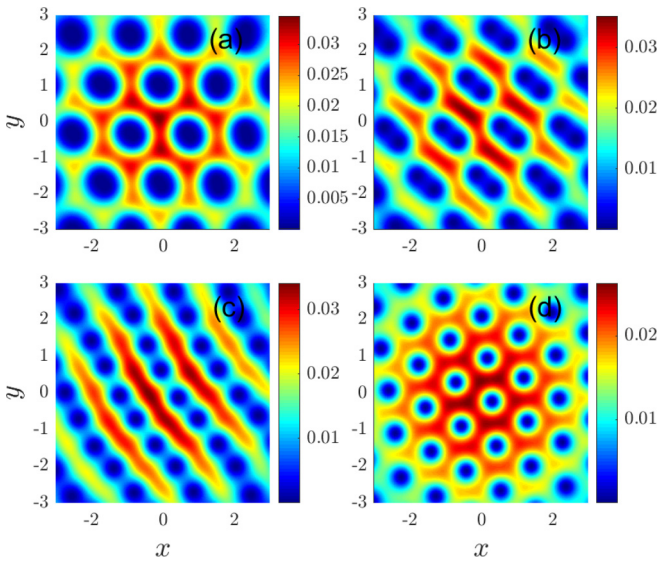

FIG. 7. Effect of contact interaction $\bar{g}$ on the vortex structures of a fast rotating 2D Rydberg-dressed condensate. $R_{\text{TF}} = 7R_c$, $\omega_\perp = 3\omega_c$, $\Omega = 0.95\omega_\perp = 2.85\omega_c$, $\bar{g}_{\text{eff}} = 1655$, and the LHY correction $\bar{\gamma} = 260$ are used in all frames. All axes are in units of R_c. Upon increasing $\bar{g}$, it exhibits (a) clustering of paired vortices in a hexagonal structure ($\bar{g} = 10$ and $\bar{\alpha} = 432.9$), (b) paired vortices in a striped structure ($\bar{g} = 15$ and $\bar{\alpha} = 431.6$), (c) striped lattice ($\bar{g} = 20$ and $\bar{\alpha} = 430.3$), and (d) hexagonal lattice ($\bar{g} = 140$ and $\bar{\alpha} = 398.7$).

Once $\bar{\gamma}$ is increased further to hit the SS-SF transition, the system is in the homogeneous SF regime and the vortex lattice will be in the closed-packing hexagonal structure [Fig. 2(d)].

To see how reliable the estimated n_1 and n_2 in (17) and (18) are, we show another set of vortex structures in Fig. 4. Now we fix $\bar{g}_{\text{eff}} = 3573$ with $\bar{\alpha} = 941$ and $\bar{g} = 0$ and $R_{\text{TF}} = 6R_c$, and the frequencies are doubled, $\omega_\perp = 6\omega_c$ and $\Omega = 0.95\omega_\perp = 5.7\omega_c$. Upon increasing the LHY coupling $\bar{\gamma}$, it exhibits (a) clustering of paired vortices in a honeycomb structure ($\bar{\gamma} = 300$), (b) striped lattice ($\bar{\gamma} = 600$), (c) clustering of three vortices in a hexagonal structure ($\bar{\gamma} = 990$), and (d) hexagonal lattice ($\bar{\gamma} = 1100$). In the present case, $\mathcal{A}_{\text{LLL}} \approx 0.55$ and $\mathcal{A}_\triangle/\mathcal{A}_{\text{LLL}} \approx 1.95$. It yields $n_1 = 2$ and is the case seen in Figs. 4(a) and 4(e). Moreover, $\mathcal{A}_\square/\mathcal{A}_{\text{LLL}} \approx 3.36$ and thus $n_2 = 3$. Clustering of three vortices is indeed seen in Figs. 4(c) and 4(g). Once again, the clustering of three vortices appears in a closed-packing hexagonal structure.

Finally, one more set of vortex structures are shown in Fig. 5. In this set, we fix $\bar{g}_{\text{eff}} = 8579$ with $\bar{g} = 0$ and $\bar{\alpha} = 2260$ and $R_{\text{TF}} = 6R_c$, and the frequencies are further increased to $\omega_\perp = 9.29\omega_c$ and $\Omega = 0.95\omega_\perp = 8.82\omega_c$. Upon increasing $\bar{\gamma}$, it exhibits (a) clustering of three vortices in a honeycomb structure ($\bar{\gamma} = 1250$), (b) striped lattice ($\bar{\gamma} = 1500$), (c) clustering of four (see the white oval) or five (see the black oval) vortices in a linear structure ($\bar{\gamma} = 1805$), and (d) hexagonal lattice mixed with the striped SS ($\bar{\gamma} = 1810$). In this set of parameters, $\mathcal{A}_{\text{LLL}} \approx 0.36$ and $\mathcal{A}_\triangle/\mathcal{A}_{\text{LLL}} \approx 2.98$. It yields $n_1 = 3$ which is the case seen in Figs. 5(a) and 5(e). However, $\mathcal{A}_\square/\mathcal{A}_{\text{LLL}} \approx 5.18$ and then $n_2 = 5$, but clustering of four or five vortices in a linear structure is actually seen in Figs. 5(c) and 5(g). When the rotation frequency Ω is high and plenty of vortices occur, n_2 given by (18) becomes not too accurate.

Once $\bar{\gamma}$ is increased to hit the SS-SF transition, hexagonal vortex lattice would appear. In Fig. 5(d), we instead show the case by slightly increasing $\bar{\gamma}$ from 1805 in case (c) to 1810. One sees hexagonal vortex lattice is mixed with the striped SS. This is just to show how rich the vortex structures could be in a fast rotating 2D Rydberg-dressed condensate with the LHY correction.

To increase the readability, the results shown in Figs. 2, 4, and 5 are summarized in a "phase diagram" in Fig. 6.

C. Effect of contact interaction

Similar to the effect of LHY coupling $\bar{\gamma}$, it is known that contact interaction $\bar{g}$ can also suppress the crystallization, and the presence of it could also result in rich vortex structures. Figure 7 presents a study on the effect of the contact interaction. In particular, we focus on how the contact interaction affect the clustering of multiple vortices. By fixing the LHY coupling $\bar{\gamma}$ and $\bar{g}_{\text{eff}}$, and changing the relative magnitudes of $\bar{g}$ and $\bar{\alpha}$, it is seen that upon increasing $\bar{g}$, clustering of paired vortices in a hexagonal structure [Fig. 7(a)] is evolved into paired vortices in a striped structure [Fig. 7(b)]. Once $\bar{g}$ is increased further, it evolves into a striped lattice [Fig. 7(c)], and eventually to a hexagonal lattice [Fig. 7(d)]. These vortex structure changes occur in a small window of $\bar{g}$.

V. CONCLUDING REMARKS

In conclusion, vortex structures in a fast rotating 2D Rydberg-dressed BEC with LHY correction are investigated. In a rotating BEC of reduced dimensionality, it is found that LHY coupling can be tuned again the short- and long-range couplings. Consequently, a rich phase diagram of vortex structures can occur. Much of the results can be understood in the context of SF-SS transition. In addition, clustering of multiple vortices can form due to the trapping effect of the SS triangles and grids. We have provided estimates for the number of vortices in the clustering.

Finally, we remark on the feasibility of the possible experiments. It is not going to be an easy experiment as many techniques are required. One has to first prepare Rydberg-dressed atoms in a quasi-2D trap and then rotate the trap potential. In any event, this can be done, in principle! The parameters $R_{\rm TF}$, $\omega_\perp$, Ω, $\bar{\alpha}$, and $\bar{g}$ used are realistic to the system [25,37]. Besides, the LHY coupling $\bar{\gamma}$, which is tunable in a quasi-2D geometry, is estimated to be also realistic to the system. We really hope the experiment can be done soon.

ACKNOWLEDGMENTS

Financial support from the Ministry of Science and Technology, Taiwan (under Grant No. 108-2112-M-003-006-MY2) and the National Center for Theoretical Sciences, Taiwan are acknowledged.

APPENDIX: LATTICE CONSTANT OF TRAPPED HEXAGONAL RYDBERG-DRESSED SS

Starting from the 2D time-dependent GPE, Eq. (10), for the rotating BEC in the rotating frame,

$$i\hbar\partial_t\phi(\vec{\rho},t)=\left[-\frac{\hbar^2\nabla_\perp^2}{2m}+\bar{V}(\vec{\rho})+\int U_{\rm 2D}(\vec{\rho}-\vec{\rho}')|\phi(\vec{\rho}',t)|^2d\vec{\rho}'+\bar{\gamma}|\phi(\vec{\rho},t)|^3\right]\phi(\vec{\rho},t), \tag{A1}$$

where $\bar{V}(\vec{\rho})=m(\omega_\perp^2-\Omega^2)\rho^2/2$ and $U_{\rm 2D}(\vec{\rho}-\vec{\rho}')$ was given in (13). Now, let $\phi(\vec{\rho},t)\equiv\exp(-i\mu t/\hbar)[\phi_0(\vec{\rho})+\delta\phi(\vec{\rho},t)]$, where $\phi_0(\vec{\rho})$ satisfies the time-independent GPE,

$$\left[-\frac{\hbar^2\nabla_\perp^2}{2m}+\bar{V}(\vec{\rho})+\int U_{\rm 2D}(\vec{\rho}-\vec{\rho}')|\phi_0(\vec{\rho}')|^2d\vec{\rho}'+\bar{\gamma}|\phi_0(\vec{\rho})|^3\right]\phi_0(\vec{\rho})=\mu\phi_0(\vec{\rho}), \tag{A2}$$

and to the linear order, the fluctuation $\delta\phi(\vec{\rho},t)$ satisfies

$$\begin{aligned}i\hbar\partial_t\delta\phi(\vec{\rho},t)\simeq&\left[-\frac{\hbar^2\nabla_\perp^2}{2m}+\bar{V}(\vec{\rho})+\int U_{\rm 2D}(\vec{\rho}-\vec{\rho}')|\phi_0(\vec{\rho}')|^2d\vec{\rho}'+\bar{\gamma}|\phi_0(\vec{\rho})|^3-\mu\right]\delta\phi(\vec{\rho},t)\\&+\int U_{\rm 2D}(\vec{\rho}-\vec{\rho}')\phi_0(\vec{\rho}')\delta\phi^*(\vec{\rho}',t)d\vec{\rho}'\phi_0(\vec{\rho})+\int U_{\rm 2D}(\vec{\rho}-\vec{\rho}')\phi_0^*(\vec{\rho}')\delta\phi(\vec{\rho}',t)d\vec{\rho}'\phi_0(\vec{\rho})\\&+\frac{3\bar{\gamma}|\phi_0(\vec{\rho})|^3}{2}\delta\phi(\vec{\rho},t)+\frac{3\bar{\gamma}|\phi_0(\vec{\rho})|^3\phi_0(\vec{\rho})}{2\phi_0^*(\vec{\rho})}\delta\phi^*(\vec{\rho},t).\end{aligned} \tag{A3}$$

In the uniform limit appropriate for the region near the trap center, $\bar{V}(\vec{\rho})\to 0$, $\phi_0(\vec{\rho})\equiv\sqrt{n_0}$ is a real constant and (A2) yields $n_0\int U_{\rm 2D}(\vec{\rho}-\vec{\rho}')d\vec{\rho}'+\bar{\gamma}n_0^{3/2}=\mu$. In addition, (A3) is reduced to

$$\begin{aligned}i\hbar\partial_t\delta\phi(\vec{\rho},t)\simeq&-\frac{\hbar^2\nabla_\perp^2}{2m}\delta\phi(\vec{\rho},t)+n_0\int U_{\rm 2D}(\vec{\rho}-\vec{\rho}')\delta\phi^*(\vec{\rho}',t)d\vec{\rho}'+n_0\int U_{\rm 2D}(\vec{\rho}-\vec{\rho}')\delta\phi(\vec{\rho}',t)d\vec{\rho}'\\&+\frac{3\bar{\gamma}n_0^{3/2}}{2}\delta\phi(\vec{\rho},t)+\frac{3\bar{\gamma}n_0^{3/2}}{2}\delta\phi^*(\vec{\rho},t).\end{aligned} \tag{A4}$$

Equation (A4) can be used to study the SS state in the background of uniform density n_0. For simplicity, we consider $\delta\phi(\vec{\rho},t)$ to be a real *periodic* function with no time dependence. Thus (A4) reduces to

$$-\frac{\hbar^2\nabla_\perp^2}{2m}\delta\phi(\vec{\rho})+2n_0\int U_{\rm 2D}(\vec{\rho}-\vec{\rho}')\delta\phi(\vec{\rho}')d\vec{\rho}'+3\bar{\gamma}n_0^{3/2}\delta\phi(\vec{\rho})=0. \tag{A5}$$

The integral term in (A5) can be expanded as

$$\int U_{\rm 2D}(\vec{\rho}-\vec{\rho}')\delta\phi(\vec{\rho}')d\vec{\rho}'=\frac{1}{(2\pi)^2}\int\tilde{U}_{\rm 2D}(\mathbf{k}_\parallel)\delta\tilde{\phi}(\mathbf{k}_\parallel)e^{i\mathbf{k}_\parallel\cdot\vec{\rho}}d\mathbf{k}_\parallel=\tilde{U}_{\rm 2D}(0)\delta\phi(\vec{\rho})-\frac{\tilde{U}''_{\rm 2D}(0)}{2!}\nabla_\perp^2\delta\phi(\vec{\rho})+\cdots, \tag{A6}$$

where $\tilde{U}_{\rm 2D}(\mathbf{k}_\parallel)$ and $\delta\tilde{\phi}(\mathbf{k}_\parallel)$ are Fourier transforms of $U_{\rm 2D}(\vec{\rho})$ and $\delta\phi(\vec{\rho})$. Keeping up to second-order terms in Fourier expansion, (A5) can be approximated by

$$\left[-\frac{\hbar^2}{4m}-\frac{\tilde{U}''_{\rm 2D}(0)n_0}{2!}\right]\nabla_\perp^2\delta\phi(\vec{\rho})+\left[n_0\tilde{U}_{\rm 2D}(0)+\frac{3\bar{\gamma}n_0^{3/2}}{2}\right]\delta\phi(\vec{\rho})=0. \tag{A7}$$

Recall in (12) that $\tilde{U}_{2D}(0) \equiv \bar{g}_{\rm eff} = \bar{g} + 2\pi^2\bar{\alpha}/3\sqrt{3}R_c^4$ and $\tilde{U}''_{2D}(0) = -\pi^2\bar{\alpha}/6\sqrt{3}R_c^2$. Consequently, (A7) can be rewritten as

$$\nabla_\perp^2 \delta\phi(\vec{\rho}) + \mathcal{K}^2 \delta\phi(\vec{\rho}) = 0, \tag{A8}$$

where

$$\mathcal{K}^2 = \frac{4}{R_c^2}\left(1 + \frac{3\bar{\gamma} n_0^{\frac{1}{2}}}{2\bar{g}_{\rm eff}}\right)\left[\frac{mn_0R_c^2(\bar{g}_{\rm eff} - \bar{g}) - 2\hbar^2}{mn_0R_c^2\bar{g}_{\rm eff}}\right]^{-1}, \tag{A9}$$

and under Thomas-Fermi approximation, the background density n_0 can be approximated as

$$n_0 = m(\omega_\perp^2 - \Omega^2)R_{\rm TF}^2/2\bar{g}_{\rm eff}. \tag{A10}$$

Now we consider the SS with a hexagonal structure, such as those shown in Figs. 2(a), 4(a), and 5(a). Subject to the constraint of a circular trap, when one picks a SS droplet near the center as the origin, the nearby six droplets all have a distance a from the center. In other words, they are all located in the circumference of a circle with radius a. Connecting the origin with any nearby droplet at $\vec{\rho}$, the periodic density modulation along that direction should behave as

$$|\delta\phi(\vec{\rho})|^2 \propto \cos^2(k\rho) \quad \text{with} \quad k = \frac{\pi}{a} \quad \text{and} \quad \rho = |\vec{\rho}|. \tag{A11}$$

Substitution of (A11) into (A8), one obtains $\mathcal{K}^2 = k^2 = (\pi/a)^2$, or

$$a = \frac{\pi}{\mathcal{K}} = \frac{\pi R_c}{2}\left(1 + \frac{3\bar{\gamma} n_0^{\frac{1}{2}}}{2\bar{g}_{\rm eff}}\right)^{-\frac{1}{2}}\left[\frac{mn_0R_c^2(\bar{g}_{\rm eff} - \bar{g}) - 2\hbar^2}{mn_0R_c^2\bar{g}_{\rm eff}}\right]^{\frac{1}{2}}. \tag{A12}$$

The parameters used in Figs. 2, 4, and 5 all fulfill $a \approx \pi R_c/2$.

[1] A. A. Abrikosov, Sov. Phys. JETP **5**, 1174 (1957).
[2] A. A. Abrikosov, Rev. Mod. Phys. **76**, 975 (2004).
[3] E. L. Andronikashvili and Y. G. Mamaladze, Rev. Mod. Phys. **38**, 567 (1966).
[4] M. M. Salomaa and G. E. Volovik, Rev. Mod. Phys. **59**, 533 (1987).
[5] P. C. Haljan, I. Coddington, P. Engels, and E. A. Cornell, Phys. Rev. Lett. **87**, 210403 (2001).
[6] J. R. Abo-Shaeer, C. Raman, J. M. Vogels, and W. Ketterle, Science **292**, 476 (2001).
[7] Y. Li, A. Geißler, W. Hofstetter, and W. Li, Phys. Rev. A **97**, 023619 (2018).
[8] S. Saccani, S. Moroni, and M. Boninsegni, Phys. Rev. Lett. **108**, 175301 (2012).
[9] M. Kunimi and Y. Kato, Phys. Rev. B **86**, 060510(R) (2012).
[10] T. Macrì, F. Maucher, F. Cinti, and T. Pohl, Phys. Rev. A **87**, 061602(R) (2013).
[11] F. Ancilotto, M. Rossi, and F. Toigo, Phys. Rev. A **88**, 033618 (2013).
[12] T. Macrì, S. Saccani, and F. Cinti, J. Low Temp. Phys. **177**, 59 (2014).
[13] A. Putra, F. Salces-Cárcoba, Y. Yue, S. Sugawa, and I. B. Spielman, Phys. Rev. Lett. **124**, 053605 (2020).
[14] D. Petter, G. Natale, R. M. W. van Bijnen, A. Patscheider, M. J. Mark, L. Chomaz, and F. Ferlaino, Phys. Rev. Lett. **122**, 183401 (2019).
[15] G. Natale, R. M. W. van Bijnen, A. Patscheider, D. Petter, M. J. Mark, L. Chomaz, and F. Ferlaino, Phys. Rev. Lett. **123**, 050402 (2019).
[16] L. Chomaz, D. Petter, P. Ilzhöfer, G. Natale, A. Trautmann, C. Politi, G. Durastante, R. M. W. van Bijnen, A. Patscheider, M. Sohmen, M. J. Mark, and F. Ferlaino, Phys. Rev. X **9**, 021012 (2019).
[17] J.-R. Li, J. Lee, W. Huang, S. Burchesky, B. Shteynas, F. Ç. Top, A. O. Jamison, and W. Ketterle, Nature (London) **543**, 91 (2017).
[18] J. Leonard, A. Morales, P. Zupancic, T. Esslinger, and T. Donner, Nature (London) **543**, 87 (2017).
[19] L. Tanzi, J. G. Maloberti, G. Biagioni, A. Fioretti, C. Gabbanini, and G. Modugno, arXiv:1912.01910.
[20] I. Ferrier-Barbut, H. Kadau, M. Schmitt, M. Wenzel, and T. Pfau, Phys. Rev. Lett. **116**, 215301 (2016).
[21] F. Cinti, A. Cappellaro, L. Salasnich, and T. Macrì, Phys. Rev. Lett. **119**, 215302 (2017).
[22] N. Henkel, R. Nath, and T. Pohl, Phys. Rev. Lett. **104**, 195302 (2010).
[23] G. Pupillo, A. Micheli, M. Boninsegni, I. Lesanovsky, and P. Zoller, Phys. Rev. Lett. **104**, 223002 (2010).
[24] F. Cinti, P. Jain, M. Boninsegni, A. Micheli, P. Zoller, and G. Pupillo, Phys. Rev. Lett. **105**, 135301 (2010).
[25] C.-H. Hsueh, T.-C. Lin, T.-L. Horng, and W. C. Wu, Phys. Rev. A **86**, 013619 (2012).
[26] C.-H. Hsueh, Y.-C. Tsai, K.-S. Wu, M.-S. Chang, and W. C. Wu, Phys. Rev. A **88**, 043646 (2013).
[27] T. D. Lee, K. Huang, and C. N. Yang, Phys. Rev. **106**, 1135 (1957).
[28] A. Cidrim, F. E. A. dos Santos, E. A. L. Henn, and T. Macrì, Phys. Rev. A **98**, 023618 (2018).
[29] A. R. P. Lima and A. Pelster, Phys. Rev. A **84**, 041604(R) (2011).
[30] S. Gautam and S. K. Adhikari, Ann. Phys. **409**, 167917 (2019).
[31] A. Boudjemâa, Phys. Rev. A **98**, 033612 (2018).

[32] Y.-C. Zhang, F. Maucher, and T. Pohl, Phys. Rev. Lett. **123**, 015301 (2019).
[33] F. Böttcher, J.-N. Schmidt, M. Wenzel, J. Hertkorn, M. Guo, T. Langen, and T. Pfau, Phys. Rev. X **9**, 011051 (2019).
[34] L. Tanzi, E. Lucioni, F. Famà, J. Catani, A. Fioretti, C. Gabbanini, R. N. Bisset, L. Santos, and G. Modugno, Phys. Rev. Lett. **122**, 130405 (2019).
[35] I. Seydi, S. H. Abedinpour, R. E. Zillich, R. Asgari, and B. Tanatar, Phys. Rev. A **101**, 013628 (2020).
[36] G. McCormack, R. Nath, and W. Li, Phys. Rev. A **102**, 023319 (2020).
[37] N. Henkel, F. Cinti, P. Jain, G. Pupillo, and T. Pohl, Phys. Rev. Lett. **108**, 265301 (2012).
[38] S.-C. Cheng and S.-D. Jheng, Sci. Rep. **6**, 31801 (2016).
[39] M. P. Kwasigroch and N. R. Cooper, Phys. Rev. A **86**, 063618 (2012).
[40] R. K. Kumar, L. Tomio, B. A. Malomed, and A. Gammal, Phys. Rev. A **96**, 063624 (2017).
[41] M. N. Tengstrand, P. Stürmer, E. O. Karabulut, and S. M. Reimann, Phys. Rev. Lett. **123**, 160405 (2019).
[42] R. Tamil Thiruvalluvar, S. Sabari, K. Porsezian, and P. Muruganandam, Physica E: Low-dimensional Syst. Nanostruct. **107**, 54 (2019).
[43] S. M. Roccuzzo, A. Gallemí, A. Recati, and S. Stringari, Phys. Rev. Lett. **124**, 045702 (2020).
[44] A. Gallemí, S. M. Roccuzzo, S. Stringari, and A. Recati, Phys. Rev. A **102**, 023322 (2020).
[45] J. Sinova, C. B. Hanna, and A. H. MacDonald, Phys. Rev. Lett. **89**, 030403 (2002).
[46] C. J. Pethick and H. Smith, *Bose-Einstein Condensation in Dilute Gases* (Cambridge University Press, Cambridge, 2002).
[47] C. Van Loan, *Computational Frameworks for the Fast Fourier Transform* (Society for Industrial and Applied Mathematics, Philadelphia, 1992).
[48] K. Kasamatsu, M. Tsubota, and M. Ueda, Phys. Rev. Lett. **91**, 150406 (2003).
[49] M. Ueda, *Fundamentals and New Frontiers of Bose-Einstein Condensation* (World Scientific Publishing, Singapore, 2010).